View metadata, citation and similar papers at core.ac.uk

brought to you by CORE

provided by Portsmouth University Research Portal (Pure)

MNRAS **466,** 4021–4028 (2017)
Advance Access publication 2017 January 7

doi:10.1093/mnras/stw3375

Deep *Chandra* observations of NGC 7457, the X-ray point source populations of a low-mass early-type galaxy

Mark B. Peacock,[1]★ Stephen E. Zepf,[1] Arunav Kundu,[2] Thomas J. Maccarone,[3] Bret D. Lehmer,[4] Anthony H. Gonzalez[5] and Claudia Maraston[6]

[1]*Department of Physics and Astronomy, Michigan State University, East Lansing, MI 48824, USA*
[2]*Eureka Scientific, Inc., 2452 Delmer Street, Suite 100, Oakland, CA 94602, USA*
[3]*Physics Department, Texas Tech University, PO Box 41051, Lubbock, TX 79409, USA*
[4]*Department of Physics, University of Arkansas, 226 Physics Building, 835 West Dickson Street, Fayetteville, AR 72701, USA*
[5]*Department of Astronomy, University of Florida, Gainesville, FL 32611, USA*
[6]*Institute of Cosmology and Gravitation, Dennis Sciama Building, Burnaby Road, Portsmouth PO1 3FX, UK*

Accepted 2016 December 23. Received 2016 December 20; in original form 2016 October 24

ABSTRACT

We present the X-ray point source population of NGC 7457 based on 124 ks of *Chandra* observations. Previous deep *Chandra* observations of low-mass X-ray binaries (LMXBs) in early-type galaxies have typically targeted the large populations of massive galaxies. NGC 7457 is a nearby, early-type galaxy with a stellar luminosity of $1.7 \times 10^{10}\,L_{K\odot}$, allowing us to investigate the populations in a relatively low-mass galaxy. We classify the detected X-ray sources into field LMXBs, globular cluster LMXBs and background active galactic nuclei based on identifying optical counterparts in new *HST*/ACS images. We detect 10 field LMXBs within the r_{ext} ellipse of NGC 7457 (with semimajor axis ∼9.1 kpc, ellipticity = 0.55). The corresponding number of LMXBs with X-ray luminosities (L_x) $> 2 \times 10^{37}$ erg s^{-1} per stellar luminosity is consistent with that observed in more massive galaxies, ∼7 per $10^{10}\,L_{K\odot}$. We detect a small globular cluster population in these *HST* data and show that its colour distribution is likely bimodal and that its specific frequency is similar to that of other early-type galaxies. However, no X-ray emission is detected from any of these clusters. Using published data for other galaxies, we show that this non-detection is consistent with the small stellar mass of these clusters. We estimate that 0.11 (and 0.03) LMXBs are expected per $10^6\,M_{\odot}$ in metal-rich (and metal-poor) globular clusters. This corresponds to 1100 (and 330) LMXBs per $10^{10}\,L_{K\odot}$, highlighting the enhanced formation efficiency of LMXBs in globular clusters. A nuclear X-ray source is detected, with L_x varying from 2.8×10^{38} to 6.8×10^{38} erg s^{-1}. Combining this L_x with a published dynamical mass estimate for the central supermassive black hole in NGC 7457, we find that L_x/L_{Edd} varies from 0.5×10^{-6} to 1.3×10^{-6}.

Key words: galaxies: individual: NGC 7457 – galaxies: star clusters: general – X-rays: binaries – X-rays: galaxies.

1 INTRODUCTION

The superb spatial resolution of the *Chandra* X-ray observatory has revealed large point source populations in local galaxies [see e.g. the review of Fabbiano (2006) and references therein]. For the old stellar populations of early-type galaxies, these sources are primarily thought to be low-mass X-ray binaries (LMXBs). For the closest galaxies, deep *Chandra* observations can probe the LMXB populations to X-ray luminosities (L_x) of few $\times\ 10^{37}$ erg s^{-1}, or fainter. This allows us to study a significant fraction of the active LMXB population and investigate the X-ray luminosity function (XLF), the shape of which may provide clues to the nature of the LMXB populations.

Beyond the Local Group, optical emission from LMXBs will be too faint to detect with *HST* observations. However, combining *Chandra* with optical *HST* data is powerful for identifying globular cluster LMXBs and background active galactic nuclei (AGN), by detecting their host clusters and galaxies, respectively. Such work has demonstrated that a large fraction (20–70 per cent) of the LMXBs observed in nearby early-type galaxies are located in their globular clusters (e.g. Angelini, Loewenstein & Mushotzky 2001;

★ E-mail: mpeacock@msu.edu

© 2017 The Authors
Published by Oxford University Press on behalf of the Royal Astronomical Society

Kundu, Maccarone & Zepf 2002; Jordán et al. 2004). These globular cluster LMXBs are likely formed via dynamical interactions (e.g. Clark 1975; Verbunt & Hut 1987; Jordán et al. 2007; Peacock et al. 2009) and should therefore be treated as a distinct population from the LMXBs in the field of a galaxy (although a small fraction of field LMXBs may have originated in clusters; e.g. Kim et al. 2009).

Deep *Chandra* observations of massive early-type galaxies have previously been used for detailed studies of their LMXB populations (e.g. Brassington et al. 2008, 2009; Sivakoff et al. 2008; Voss et al. 2009; Li et al. 2010; Luo et al. 2013; Lehmer et al. 2014; Lin et al. 2015). However, the available data for lower mass early-type galaxies are significantly less deep [e.g. Coulter et al. (2016), who studied six galaxies with $L_K = (1-2) \times 10^{10}\,\mathrm{L_{K\odot}}$ but with relatively bright detection limits of $L_x > 1 \times 10^{38}\,\mathrm{erg\,s^{-1}}$]. In this paper, we present the field LMXB population of NGC 7457 based on deep *Chandra* observations. This is a nearby ($d = 12.1$ Mpc; Tully et al. 2013) early-type galaxy (S0; de Vaucouleurs et al. 1991) that has a relatively low mass, with a velocity dispersion of $75\,\mathrm{km\,s^{-1}}$ (Cappellari et al. 2013) and *K*-band luminosity of $1.7 \times 10^{10}\,\mathrm{L_{K\odot}}$ (Jarrett et al. 2003). It also has a central supermassive black hole (SMBH) with dynamical mass estimates that suggests that it has relatively low mass ($M_{\mathrm{BH}} = 4.1^{+1.2}_{-1.7} \times 10^6\,\mathrm{M_\odot}$; Gebhardt et al. 2003; Gültekin et al. 2009), consistent with the galaxy's low stellar mass.

We present these new *Chandra* observations of NGC 7457 and the detected X-ray populations in Section 2. In Section 3, we present *HST* observations of the galaxy, which we use to identify and study globular cluster candidates and classify sources into field LMXBs, globular cluster LMXBs and background AGN. In Sections 4 and 5, we discuss the observed field and globular cluster LMXB populations and compare them with those observed in other, more massive early-type galaxies. In Section 6, we discuss the observed nuclear emission, before concluding in Section 7.

2 *CHANDRA* OBSERVATIONS AND REDUCTION

Chandra has observed NGC 7457 with the Advanced CCD Imaging Spectrometer (ACIS) on three epochs under proposal numbers 11900514 [PI Gultekin, see Gültekin et al. (2012)] and 16620677 (PI Peacock). We utilize these three observations: Obs ID 11786, 29 ks obtained on 2009 September 11; Obs ID 17007, 45 ks obtained on 2015 September 11; and Obs ID 18440, 51 ks obtained on 2015 September 17.

We reduce and analyse these data using the CHANDRA INTERACTIVE ANALYSIS OF OBSERVATIONS (CIAO) software (Fruscione et al. 2006). All three observations are reprocessed using the CHANDRA_REPRO script. We use DMEXTRACT to extract the counts in background regions of these 'evt' files. This identifies no flaring events in the three observations. All three observations have similar aimpoints (within 3 arcsec). We utilize only the data from the back illuminated S3 chip, which encloses the entire r_{ext}[1] ellipse of the galaxy.

Before analysing these data, we align the different observations with a common reference system. To do this, we use FLUX-IMAGE to produce exposure corrected images in the energy range 0.5–7.0 keV and MKPSFMAP to produce psf maps with an effective energy of 2.3 keV and an enclosed counts fraction of 0.9. Sources are identified in these broad-band images using WAVDETECT with *scales* = 1, 2, 4, 6, 8, 12, 16, 24 and 32 and detection threshold, $sigthresh = 10^{-6}$. We select only well-centred sources by requiring that the sources have $counts > 10$ and $psf\_size < 7$ pixels. The three observations are aligned with the longest exposure observation (Obs ID 18 440) using WCS_MATCH to calculate the transformations. The derived shifts (Δra, Δdec) are 0.09 arcsec, 0.41 arcsec for Obs ID 11786 and 0.44 arcsec, 0.23 arcsec for Obs ID 17 707. These are applied to the event files (evt2) and aspect solutions (asol) using WCS_UPDATE.

Exposure corrected images in the *Chandra* source catalogue's broad-band (0.5−7.0 keV) are produced for the individual observations and the combined aligned data using MERGE_OBS. These images are created with $binsize = 1$ and hence maintain the native pixel size of 0.492 arcsec. Point spread function (PSF) maps are created for the individual observations using MKPSFMAP with an effective energy of 2.3 keV and an enclosed counts fraction of 0.9. Such a map cannot be constructed directly from the combined image. Instead, we construct a combined PSF map as an exposure weighted sum of the individual observation PSF maps. Sources are detected in the individual and combined observations using WAVDETECT with *scales* = 1, 2, 4, 6, 8, 12, 16, 24 and 32 and detection threshold, $sigthresh = 10^{-6}$. The combined 124.3-ks data set reaches a (on-axis) detection limit[2] of $L_x \sim 1 \times 10^{37}\,\mathrm{erg\,s^{-1}}$. We identify 16 sources within the r_{ext} ellipse of NGC 7457. No transients are identified in the individual images that are not recovered in the combined image.

For all of the WAVDETECT locations, source fluxes are extracted from circular regions enclosing 90 per cent of the energy at 2.3 keV. Background regions are defined as an annulus 2–10 times the source radius. These regions are created using PSFSIZE_SRCS and ROI, which also exclude other sources located in the background regions. We use these regions and the task SRCFLUX to determine the net counts and fluxes at the locations of each source in the combined data and in each of the three observations. Within this task, we use the arfcorr method to model the PSF and calculate the enclosed energy fraction for both the source and background regions. SRCFLUX also uses MODELFLUX to determine unabsorbed model fluxes for each source. We correct for Galactic N_{H},[3] assuming a single value of $5.5 \times 10^{20}\mathrm{cm^{-2}}$. Most sources have very few counts; we therefore model the flux from all sources as a single power law with a photon index of 1.6. Finally, we convert fluxes to luminosities, assuming a distance to NGC 7457 of 12.1 Mpc (Tully et al. 2013).

To measure faint sources and improve the signal-to-noise ratio, we also require source fluxes measured from the combined data set. However, we cannot simply obtain these by running SRCFLUX on the combined event file. Instead, we choose to produce combined fluxes by combining the results from our individual analyses. For each source, we use SPECTRA_COMBINE to combine the pulse invariant ('pi') and response ('nopsf.arf') files produced for each source and calculate the exposure weighted net count rate from the individual 'NET_RATE_APER' values determined by SRCFLUX. We then use MODELFLUX with these combined arf files, rmf files and weighted net count rates to determine the unabsorbed model fluxes, assuming the same models and N_{H} discussed above. Uncertainties on the combined flux are calculated by propagating the errors on the individual observations.

[1] The r_{ext} ellipse is the 'total' aperture defined in the 2MASS large galaxy atlas; see Jarrett et al. (2003) for details. It is a similar scale to the optical D25 ellipse. For NGC 7457, this ellipse has semimajor axis =155 arcsec ∼ 9.1 kpc and ellipticity = 0.55.

[2] Based on detecting eight counts and estimated using http://cxc.harvard.edu/toolkit/pimms.jsp.

[3] Obtained from http://cxc.harvard.edu/toolkit/colden.jsp for the centre of the NGC 7457 (23 00 59.9, +30 08 42.0).

Table 1. Detected sources X-ray sources within $r_{\rm ext}$.

			OBS ID 11786		OBS ID 17007		OBS ID 18440		COMBINED			
ID	RA	DEC	RATE[a]	L_x[b]	RATE[a]	L_x[b]	RATE[a]	L_x[b]	RATE[a]	L_x[b] (+/−err)	R_{gcp}[c]	$f^d_{\rm opt}$
01*	345.2496621	30.1448416	16.7	2.39	40.5	7.24	33.8	6.04	32.3	5.46 + 0.50 −0.49	0.2	Nuc.
02	345.2509550	30.1463913	1.4	0.20	1.1	0.20	0.3	0.06	0.8	0.14 + 0.11 −0.06	6.8	<10 arcsec
03	345.2449162	30.1428012	1.5	0.21	1.5	0.26	1.2	0.22	1.4	0.23 + 0.13 −0.08	16.5	no
04	345.2549238	30.1500442	12.7	1.90	11.9	2.32	16.8	3.15	14.1	2.53 + 0.34 −0.33	24.8	no
05	345.2419307	30.1472114	6.5	0.93	6.0	1.07	6.8	1.21	6.4	1.09 + 0.24 −0.19	25.4	no
06	345.2464571	30.1519551	6.9	0.99	3.2	0.57	2.8	0.50	3.9	0.66 + 0.19 −0.14	27.3	no
07	345.2613643	30.1405110	0.7	0.10	1.4	0.28	1.5	0.26	1.3	0.22 + 0.13 −0.08	39.8	no
08	345.2654915	30.1451776	3.4	0.49	0.0	0.00	0.0	0.00	1.2	0.20 + 0.08 −0.05	49.4	no
09	345.2658659	30.1370842	1.4	0.21	0.9	0.17	0.6	0.10	0.9	0.15 + 0.11 −0.06	57.8	no
10	345.2550423	30.1656542	2.2	0.32	0.2	0.03	0.4	0.07	0.7	0.13 + 0.10 −0.05	76.6	yes
11	345.2666487	30.1249590	0.3	0.04	0.4	0.07	1.4	0.26	0.8	0.14 + 0.10 −0.06	89.2	no
12	345.2199592	30.1481165	1.5	0.21	3.2	0.58	2.8	0.51	2.6	0.45 + 0.17 −0.12	93.1	yes
13	345.2698244	30.1239772	5.7	0.83	1.1	0.21	2.1	0.38	2.6	0.45 + 0.16 −0.11	98.1	yes
14	345.2170819	30.1511690	1.8	0.27	0.4	0.13	1.9	0.42	1.4	0.30 + 0.16 −0.10	103.8	no
15	345.2216308	30.1636408	0.7	0.10	0.4	0.07	1.0	0.19	0.7	0.12 + 0.11 −0.06	110.2	no
16	345.2878914	30.1178499	1.0	0.15	5.2	0.98	3.8	0.71	3.7	0.65 + 0.20 −0.16	153.8	yes

Notes. [a]Net count rate ($\times 10^{-4}$ counts s^{-1}).
[b]Broad-band luminosity ($\times 10^{38}$ erg s^{-1}). Assumes a power law with a photon index, $\Gamma = 1.6$, and a distance to NGC 7457 of 12.1 Mpc.
[c]Projected distance from the centre of the galaxy (arcsec).
[d]Indicates whether the source has an optical counterpart in the *HST* F475W and/or F850LP images.
*Source 01 is the nuclear source; its L_x measurements are based on fitting its spectra (rather than assuming $\Gamma = 1.6$, see Section 6).

The detected sources, their count rates and luminosities are listed in Table 1.

3 *HST* OBSERVATIONS

The X-ray sources detected within the $r_{\rm ext}$ ellipse of NGC 7457 are likely to be a combination of LMXBs in the field of the galaxy, LMXBs within its globular clusters, and contamination from background AGN/foreground stars. We can distinguish between these sources by identifying optical counterparts to globular cluster sources and background AGN. To do this, we utilize *HST* Advanced Camera for Surveys (ACS) observations of the galaxy. A 2×1 mosaic, which covers the entire $r_{\rm ext}$ ellipse of NGC 7457, was obtained on 2014 December 11 (program ID 13942; PI Peacock). The two fields were observed through the F475W and F850LP filters (similar to the ground-based *g*- and *z*-bands), with total exposure times of 2204 s and 2100 s, respectively. These *HST* images and the *Chandra* ACIS-S3 broad-band image are shown in Fig. 1. Detected X-ray sources are highlighted. It can be seen that some X-ray sources appear to be aligned with optical sources (magenta circles in Fig. 1).

We utilize the pipeline reduced 'flc' images, downloaded from the MAST archive.[4] We align these images with a common reference frame using the DRIZZLEPAC task TWEAKREG and combine the four observations through each filter to produce a stacked mosaicked image using ASTRODRIZZLE. The two mosaicked images are then aligned with the *Chandra* source catalogue by matching seven sources (including five outside of $r_{\rm ext}$) to optical counterparts using the IRAF task MSCTPEAK. The galaxy light is subtracted from these images using the IRAF task RMEDIAN, which applies a ring median filter to the images with inner and outer radii of 30 and 31 pixels, respectively. Photometry is performed on these background subtracted images through an aperture with a radius of 0.25 arcsec using SEXTRACTOR (Bertin & Arnouts 1996). Aperture corrections from 0.25 to 0.5 arcsec are calculated by comparing photometry through such apertures for bright sources. An additional correction from 0.5 arcsec to ∞ is applied based on the corrections presented by Bohlin (2011). The resulting F475W and F850LP catalogues are combined using TOPCAT (Taylor 2006).

[4] archive.stsci.edu

3.1 NGC 7457's globular clusters

NGC 7457 is known to host a small globular cluster system, estimated at 210 ± 30 clusters (Hargis et al. 2011). A sample of these clusters has been spectroscopically confirmed and studied (Chomiuk, Strader & Brodie 2008; Pota et al. 2013). A comprehensive analysis of this globular cluster system is beyond the scope of this study. However, we do wish to identify globular clusters in these *HST* data in order to classify globular cluster LMXBs. In this section, we therefore present our cluster selection criteria and give a brief discussion of their properties.

To identify globular cluster candidates from this *HST* photometry, we require that they: (1) have $-11.5 < M_{\rm F850LP} < -6.5$, which corresponds to stellar masses of $4 \times 10^4 \lesssim M_\star \lesssim 4 \times 10^6$ M$_\odot$ [assuming M$_{z\odot} = 4.5$ and $M_\star/L_z = 1.7 M_\odot/{\rm L}_{z\odot}$, based on the models of Maraston 2005 for a 12 Gyr population with $[Z/H] = -1.35$ and a Kroupa initial mass function (IMF)]; (2) have $0.6 <$ F475W-F850LP < 1.7, as observed in other globular cluster systems (e.g. Peng et al. 2006; Strader et al. 2006); (3) are extended, with CLASS_STAR < 0.9 and F850LP(0.1 arcsec) − F850LP(0.2 arcsec) > 0.5; (4) they are not too extended to be a cluster at this distance, with F850LP(0.25 arcsec) − F850LP(0.5 arcsec) < 0.6. Fig. 2 shows these selection criteria and all sources detected in the radial region 10 arcsec $< r < r_{\rm ext}$ (grey points). We have highlighted the previously proposed globular cluster candidates that have been spectroscopically confirmed by Chomiuk et al. (2008, red squares) and Pota et al. (2013, blue circles). All of these spectroscopic clusters are detected, although one is located in the noisier chip gap region of our F850LP photometry, and its properties are significantly affected by a cosmic ray. The other spectroscopic clusters are all classified as globular clusters by our analysis.

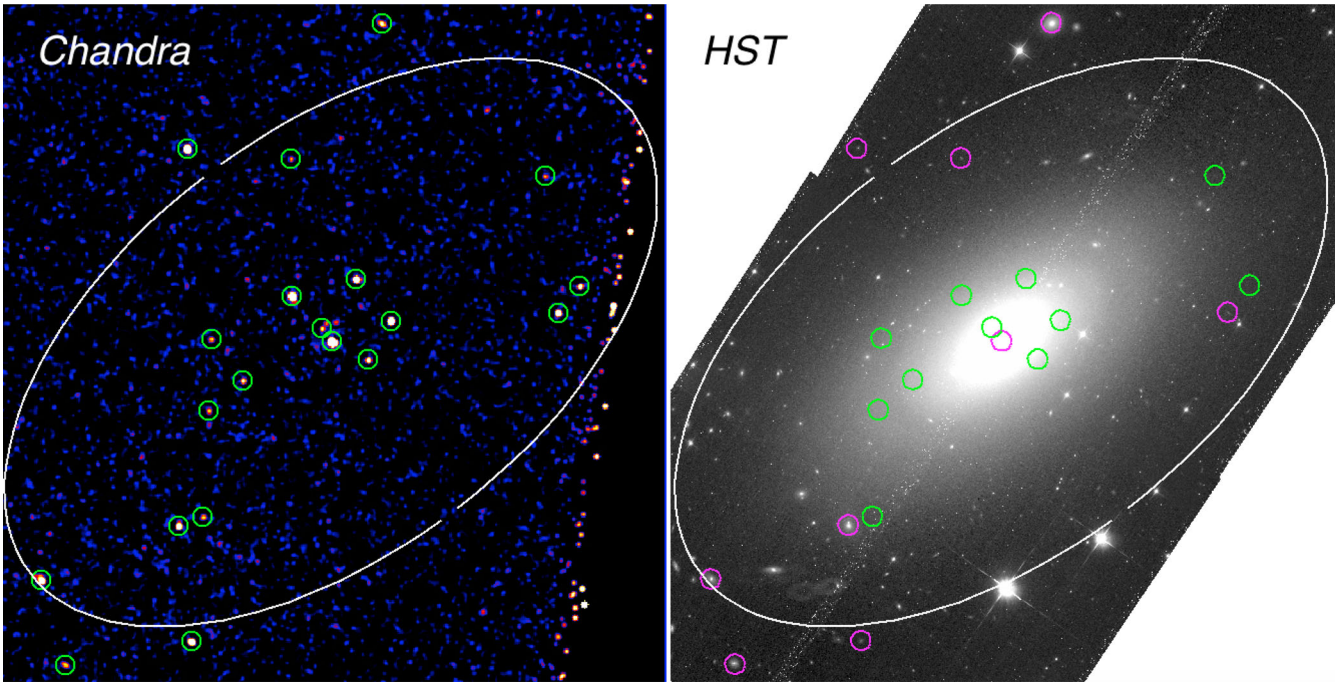

Figure 1. Left: merged *Chandra* broad-band ACIS-S image of NGC 7457. The green circles show all of the sources detected by wavdetect. Right: 2 × 1 *HST*/ACS F850LP optical mosaic of NGC 7457. The magenta and green circles indicate the locations of X-ray sources with and without optical counterparts, respectively. In both frames, the white line is the $r_{\rm ext}$ ellipse of the galaxy, to which we restrict our analysis. This ellipse has a semimajor axis = 155 arcsec ∼ 9.1 kpc and an ellipticity = 0.55. We note that the four X-ray sources outside of this ellipse have optical counterparts and are likely background AGN.

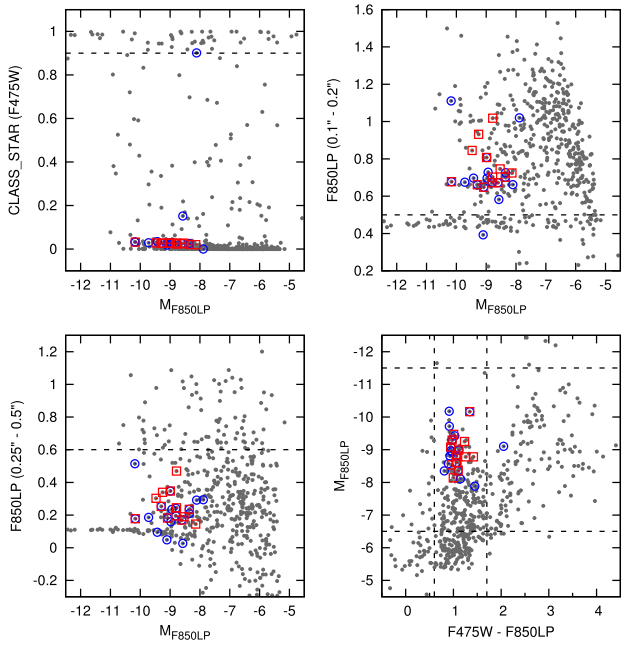

Figure 2. Properties of all sources detected in these F475W and F850LP images (grey points). The dashed black lines indicate our globular cluster selection criteria. The properties of sources previously identified as globular clusters from spectroscopic observations are highlighted with red squares and blue circles. See Section 3.1 for details.

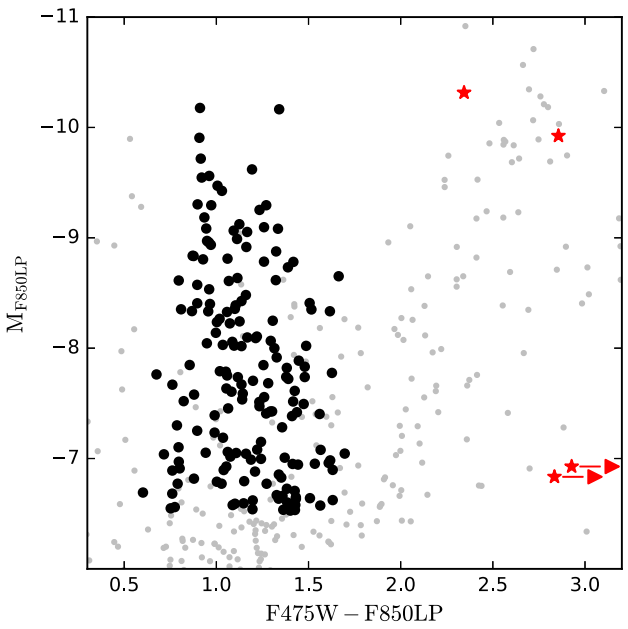

Figure 3. Colour–magnitude diagram of optical sources identified within the $r_{\rm ext}$ ellipse of NGC 7457. Globular cluster candidates are highlighted as solid black circles. The red stars show sources with X-ray emission. The red colours of these X-ray sources are consistent with them being background galaxies.

In Fig. 3, we present the observed CMD of all sources (grey points) and our globular cluster candidates (black points). We identify 65 globular cluster candidates with $M_{\rm F850LP} < -8.0$. We estimate the total number of clusters in our radial region by binning these 65 clusters into 0.5-mag bins and fitting the luminosity function to a lognormal distribution. Because of the small number of clusters, we fix the peak of the distribution at $M_{\rm F850LP} = -8.46$ and the dispersion at 0.87 [consistent with the GCLF study of

Villegas et al. (2010)]. We calculate a total of 121 globular clusters in 10 arcsec $< r < r_{\rm ext}$. This corresponds to a mass scaled specific frequency of globular clusters (e.g. Zepf & Ashman 1993), $T = N_{\rm GC}/(M_\star/10^9\,{\rm M}_\odot) = 9.5$. We take the stellar mass covered by our study to be $M_\star = 12.8 \times 10^9\,{\rm M}_\odot$, derived from the K-band light covered (calculated as 90 per cent of the total L_K based on the 2MASS LGA images; Jarrett et al. 2003) by assuming $M_\star/L_K = 0.85$ (Fall & Romanowsky 2013). We note that this is significantly larger than the value derived by Hargis et al. (2011). This is primarily due to their use of a large $M_\star/L_V$, which predicts a significantly higher mass for the galaxy. We use the K-band derived mass since the variation in $M_\star/L_K$ is known to be relatively small (e.g. Bell & de Jong 2001). This T is also directly comparable to that previously determined for more massive galaxies by Peacock & Zepf (2016), who found $5 < T < 30$, suggesting that the small globular cluster population is consistent with the galaxy's relatively low mass.

The globular cluster systems of most early-type galaxies show clear colour bimodality (e.g. Brodie & Strader 2006). However, previous studies have found no clear evidence for this in NGC 7457's clusters. Hargis et al. (2011) presented ground based $B-R$ colours of these clusters and found that they are consistent with the (bimodal) colour distribution of the Milky Way's globular clusters. However, they found no significant evidence for colour bimodality [see also Pota et al. (2013)]. Chomiuk et al. (2008) also found no significant evidence for bimodality in the $V-I$ colours of these clusters, based on the smaller area of a single WFPC2 field. We test for bimodality in the $g-z$ colours of our 65 globular cluster candidates with $M_{\rm F850LP} < -8.0$. To do this, we use the KMM test (Ashman, Bird & Zepf 1994), implemented using the GMM code of Muratov & Gnedin (2010). We run this test for two Gaussians with equal variance and obtain a best-fitting variance, $\sigma_{12} = 0.10$, and peaks in $g-z$ at $\mu_1 = 1.00$ and $\mu_2 = 1.27$. The bimodal distribution is marginally favoured, with the unimodal distribution rejected with P-value $= 0.05$. The peaks are also significantly separated with $D = (\mu_1 - \mu_2)/\sigma_{12} = 2.8$, where $D > 2$ is required to cleanly separate the two peaks (Ashman et al. 1994). The evidence for bimodality in our data may be due to our increased coverage and, hence, a larger sample size than Chomiuk et al. (2008), while the higher spatial resolution of these *HST* data may result in lower contamination from non-cluster sources than that in the study of Hargis et al. (2011). However, we caution that the bimodal case is only somewhat favoured and the number of clusters (65) is only slightly above the number required for the KMM test to be reliable (Ashman et al. 1994).

3.2 Optical counterparts to X-ray sources

Our final optical catalogue is matched to the X-ray source catalogue using TOPCAT, based on the aligned WCS and a matching radius of 0.4 arcsec. This identifies four sources within $r_{\rm ext}$ that have optical counterparts. In Fig. 4, we show F850LP cutouts for each X-ray source location. Source 01 is aligned with the centre of the galaxy. This nuclear source is discussed in Section 6. Source 02 is also close to the centre of the galaxy and is removed from our analysis because optical counterpart matching is less reliable in this inner region. It can be seen that four other sources have optical counterparts. Two have bright and extended counterparts (13 and 16). The other two have not only much fainter but also extended counterparts (10 and 12). For comparison, we also show the F850LP cut-outs of four spectroscopically confirmed globular clusters, which span the range of magnitudes studied by Chomiuk et al. (2008).

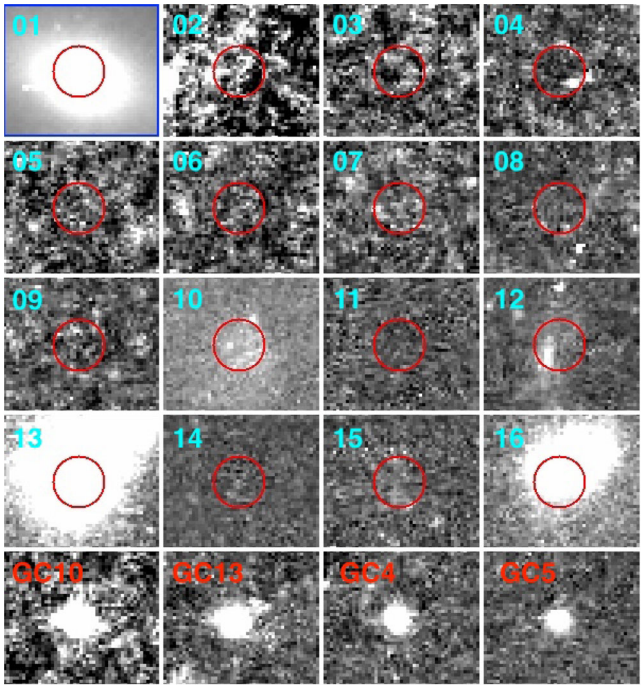

Figure 4. F850LP images at the location of each X-ray source (from top left to bottom right, sources 01−16 from Table 1). Red circles have radii = 0.4 arcsec and indicate the location of each X-ray source. For comparison, the bottom row shows four clusters from the catalogue of Chomiuk et al. (2008). From left to right, these clusters have $M_{\rm F850LP} = -10.18$, -9.72, -8.57 and -8.11. All images are background subtracted and have the same z-scale (except the central source, whose scale is adjusted to show the peak emission).

Fig. 3 shows the colour–magnitude diagram for all of our sources (grey points), our globular cluster candidates (black points) and the four sources that have X-ray counterparts (red stars). Two of the X-ray counterparts are faint and red and therefore detected only in F850LP. We plot upper limits on the colours of these sources. All four of these sources are too red to be globular clusters in NGC 7457, and they are likely to be AGN in background galaxies. These sources are flagged in Table 1 and are excluded from our analysis.

4 FIELD LMXB POPULATION

10 X-ray sources have no optical counterparts and are classified as field LMXBs in NGC 7457. In Fig. 5, we plot the luminosity of these LMXBs as a function of observation date. The blue lines show the combined luminosity and uncertainty. Only one transient is observed. Source 08 is detected in 2009 but not in the later 2015 observations.

In Fig. 6, we show the XLF of the field LMXBs identified in NGC 7457 (red points). For bright LMXBs (with $L_x > 10^{38}{\rm erg\,s^{-1}}$), we also include the average number detected in this, and five other, low-mass early-type galaxies (with $78 < \sigma < 110\,{\rm km\,s^{-1}}$; blue point). This point is taken from Coulter et al. (2016) and is based on the detection of 12 LMXBs in shallower *Chandra* observations of NGC 4339, NGC 4387, NGC 4458, NGC 4550, NGC 4551 and NGC 7457. The bright LMXB populations of these similar-mass early-type galaxies are in good agreement with NGC 7457's XLF.

We compare NGC 7457's field LMXB XLF to those published in other, more massive early-type galaxies (with $180 < \sigma < 305\,{\rm km\,s^{-1}}$; grey lines in Fig. 6). These data are taken from

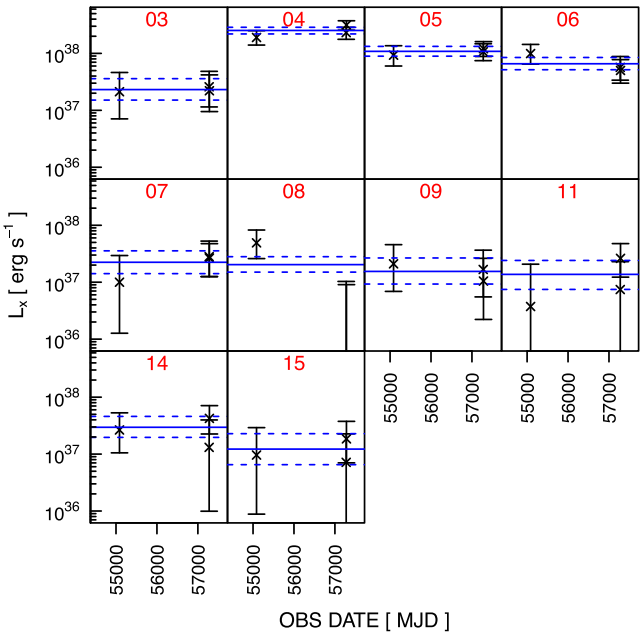

Figure 5. Luminosities of all field LMXBs detected within r_{ext}. Black points show L_x at the three epochs available. The solid (and dashed) blue lines show the average luminosity (and errors) for the combined data. The red source IDs correspond to those in Table 1. Source 08 is only detected in the first epoch; upper limits are shown for the later observations.

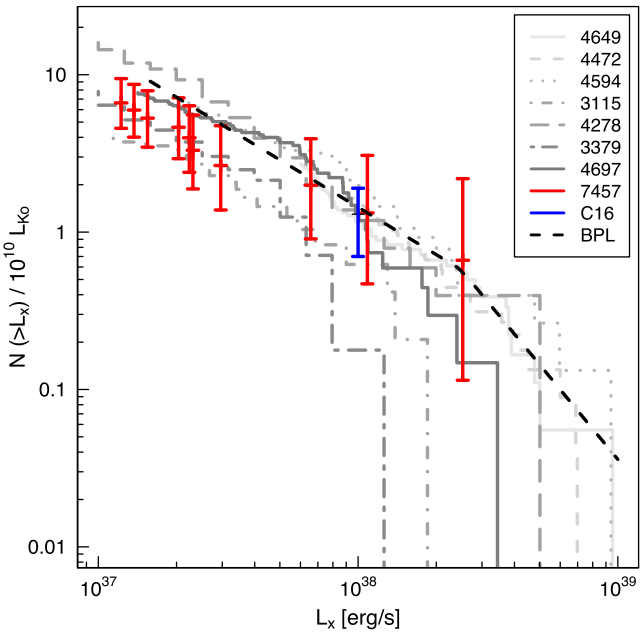

Figure 6. The cumulative XLF of field LMXBs in NGC 7457 (red points) and the average of other similar mass galaxies [from Coulter et al. (2016), C16; blue point]. They grey lines show the XLF of other, more massive early-type galaxies. Darker lines correspond to lower-velocity dispersion galaxies. The black-dotted line is the broken power law representation of the XLFs, scaled to fit all of the galaxy data.

Peacock et al. (2014) for NGC 1399, NGC 3379, NGC 4278, NGC 4472, NGC 4594, NGC 4649 and NGC 4697 and Lehmer et al. (2014) for NGC 3115. Globular cluster LMXBs and background AGN have been removed from these data in a similar way to our analysis of NGC 7457; by matching to optical counterparts in *HST* images. We scale the XLFs by the amount of *K*-band light covered based on the K_{ext} magnitude from the 2MASS LGA (Jarrett et al. 2003) and the fraction of *K*-band light covered by these X-ray catalogues [taken from Peacock et al. (2014) and Lehmer et al. (2014)]. For NGC 7457, the region studied (10 arcsec $< r < r_{ext}$) covers 90 per cent of the *K*-band light.

The black-dashed line in Fig. 6 shows a broken power law with an exponent $\alpha_1 = -1.0$ below a break at $L_x = 2.5 \times 10^{38}$erg s^{-1} and an exponent of $\alpha_2 = -2.0$ above this break. This has previously been shown to provide a good representation of the field LMXB XLF (e.g. Kim et al. 2009; Kim & Fabbiano 2010; Zhang et al. 2011; Lehmer et al. 2014; Peacock & Zepf 2016). Scaling to fit all of these galaxies, we find the number of LMXBs with $L_x > 2 \times 10^{37}$erg s^{-1} per 10^{10} L$_{K\odot}$, $n_x \sim 7$.

NGC 7457's field LMXB population is found to be similar to that of these other galaxies with $n_x = 4.6^{+2.5}_{-1.7}$. The similarity of the number of field LMXBs per L_K at all luminosities suggests a similar formation efficiency of LMXBs across these galaxies. It is worthy to note that no systematic difference is observed due to the mass of these galaxies, which span a wide range of velocity dispersions: $78 < \sigma < 305$ km s^{-1}. This suggests that factors such as primordial binary fraction and IMF do not vary significantly with galaxy mass, or that they vary in a way that does not influence LMXB formation.

5 GLOBULAR CLUSTER LMXB POPULATION

The formation of LMXBs is known to be much more efficient in globular clusters than in the fields of galaxies. Indeed, observations of other early-type galaxies have shown that large fractions of the LMXB populations are located in their globular clusters (e.g. Angelini et al. 2001; Kundu et al. 2002). Therefore, it may seem surprising that we detect no LMXBs in NGC 7457's globular clusters.

To investigate the significance of the non-detection of LMXBs in NGC 7457's clusters, we empirically predict the number of globular cluster LMXBs expected based on observations of NGC 3379, NGC 4278 and NGC 4697. Data for these galaxies were presented in Peacock et al. (2014). Their LMXB populations have been observed to follow similar detection limits to NGC 7457, and they have similar *HST* F475W and F850LP data that have been used to study their globular cluster LMXBs. We restrict the sample to clusters with $M_{F850LP} < -7.5$ and estimate the stellar mass of the clusters assuming a $M_{z\odot} = 4.50$ and a mass-to-light ratio, $M_\star/L_z = 1.7$M$_\odot$/L$_{z\odot}$ (based on the models of Maraston (2005) for a 12-Gyr population with $[Z/H] = -1.35$ and a Kroupa IMF). There is known to be an enhancement in the presence of LMXBs with metallicity (e.g. Kundu, Maccarone & Zepf 2007; Sivakoff et al. 2007; Kim et al. 2013); we therefore also split the samples into red (with F475W – F850LP > 1.2) and blue globular clusters.

We consider globular cluster LMXBs with $L_x > 2 \times 10^{37}$erg s^{-1} (all of which should be detected in these data). We find that the red (and blue) globular clusters host 0.12 (0.02), 0.11 (0.04); 0.10 (0.05) LMXBs per 10^6 M$_\odot$ in NGC 3379, NGC 4278 and NGC 4697, respectively. Therefore, on average, 0.109 and 0.033 LMXBs are expected per 10^6 M$_\odot$ in the red and blue globular clusters, respectively. To compare with the fields of these galaxies, we convert this to the number per *K*-band luminosity assuming $M_\star/L_K = 1.0$M$_\odot$/L$_{K\odot}$ [using the models of Maraston (2005), discussed above]. We find that 1090 (and 330) LMXBs are observed per 10^{10} L$_{K\odot}$ in the metal-rich (and metal-poor) globular clusters. Comparing with the number of LMXBs observed in the fields of

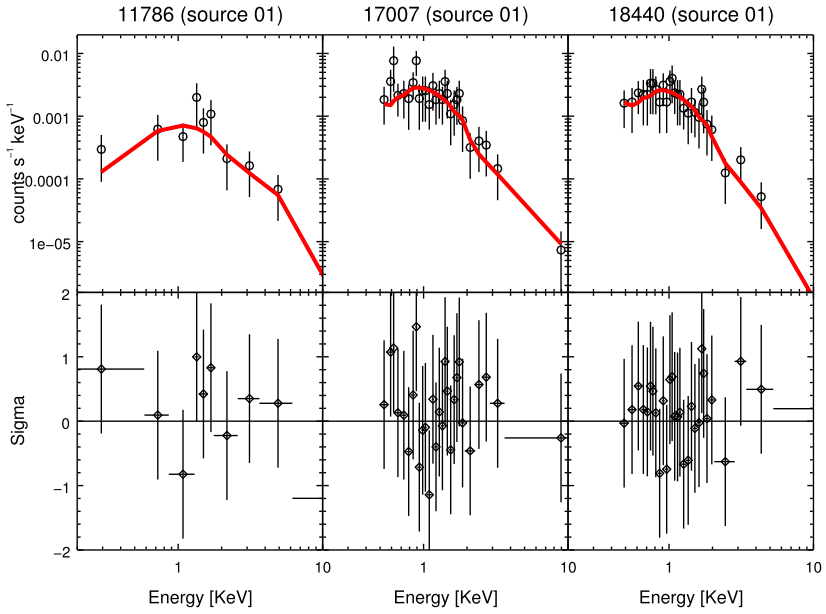

Figure 7. Top: spectra of the nuclear X-ray source in our three data sets (from left to right: 11786, 17007, 18840). Red lines show the best-fitting absorbed power-law models. Bottom: residuals for these best-fitting models.

these galaxies (4–12 per 10^{10} $L_{K\odot}$; see Section 4) highlights the enhanced formation efficiency of bright LMXBs in globular clusters.

This estimate of the number of LMXBs is based on the stellar mass of the globular clusters. In fact, we know that the dominant parameter that drives the formation of LMXBs in globular clusters is the stellar interaction rate (e.g. Verbunt & Hut 1987; Pooley et al. 2003; Peacock et al. 2009). Unfortunately, measuring this parameter for clusters beyond the Local Group is extremely challenging, as it involves resolving the clusters to their core radii. However, the mass of a cluster is correlated with the interaction rate (e.g. Davies, Piotto & de Angeli 2004; Peacock et al. 2010). Therefore, if the statistical sample is large enough, the number of LMXBs should scale with the stellar mass.

As discussed in Section 3.1, the number of globular clusters in NGC 7457 is quite small, consistent with the relatively low mass of the galaxy. We detect 99 globular clusters with $M_{\rm F850LP} < -7.5$. Assuming $M_\star/L_z = 1.7 M_\odot/L_{z\odot}$ (see above), these red (and blue) globular clusters have a total stellar mass of 9.0×10^6 $M_\odot$ (and 21.4×10^6 $M_\odot$). From the average numbers of LMXBs per stellar mass, calculated above, this predicts that NGC 7457's clusters should host 1.7 LMXBs with $L_x > 2 \times 10^{37}$ erg s^{-1} or ∼3 above our detection limit of $L_x > 1 \times 10^{37}$ erg s^{-1} (based on the observed XLF of globular clusters; Kim & Fabbiano 2010; Peacock & Zepf 2016). Therefore, while a few LMXBs would be expected on average, the non-detection in these clusters is not that surprising given the small numbers involved and the uncertainty in the interaction rates of these clusters.

6 NUCLEAR X-RAY EMISSION

The brightest X-ray source in our sample (source 01 in Table 1) is well aligned with the optical centre of the galaxy. In Fig. 7, we plot the spectra of this source for the three separate observations. Each spectrum is independently fit to absorbed power law models using SHERPA. Unabsorbed model fluxes are then calculated using MODELFLUX, as in Section 2 (but using the derived photon indices, Γ). Observations 17007 and 18440 were taken at similar times and show similar properties, with $\Gamma = 2.9 \pm 0.3$ and 3.0 ± 0.3 and $L_x = (6.8 \text{ and } 5.7) \times 10^{38}$ erg s^{-1}, respectively. Observation 11786 was taken 6 yr earlier and shows harder and fainter emission, with $\Gamma = 1.5 \pm 0.5$ and $L_x = 2.8 \times 10^{38}$ erg s^{-1}.

The central SMBH in NGC 7457 is one of only a small number with direct mass determinations. From modelling of the stellar kinematics, the mass of this black hole was calculated to be $4.1^{+1.2}_{-1.7} \times 10^6$ $M_\odot$ (Gebhardt et al. 2003; Gültekin et al. 2009). From this, we estimate the Eddington luminosity, $L_{\rm Edd} \sim 1.26 \times 10^{38} M/M_\odot = 5.1 \times 10^{44}$ erg s^{-1}.

Using these data, we calculate that the ratio of X-ray luminosity (0.5–7.0 KeV band) to Eddington luminosity ($L_x/L_{\rm Edd}$) increases from 0.5×10^{-6} to 1.3×10^{-6}. We note that Gültekin et al. (2012) previously presented $L_x/L_{\rm Edd}$ based on one of these observations, 11786. Their measurement was a factor of 2 lower, although our studies do not apply a bolometric correction, so this could be due to their use of a different energy range (2–10 KeV). Interestingly, NGC 7457 has the lowest mass SMBH of the 12 galaxies in the sample of Gültekin et al. (2012) and, for the increased flux of the source in the 2015 observations, it has the highest $L_x/L_{\rm Edd}$ ratio. This is consistent with some other observations and the theory of 'down-sizing', where lower mass black holes may accrete closer to their Eddington luminosity than higher mass black holes (e.g. Gallo et al. 2010).

7 CONCLUSIONS

We investigate the X-ray populations of NGC 7457 based on deep *Chandra* observations. We identify 10 X-ray point sources in the $r_{\rm ext}$ ellipse of the galaxy that have no optical counterparts and are likely LMXBs in the field of NGC 7457. We show that this small-field LMXB population is consistent with the populations observed in other early-type galaxies, given the relatively low stellar mass of NGC 7457. We also show that its XLF is similar to that of these other (more massive) early-type galaxies, both in shape and in scale. Our results suggest a similar formation efficiency of LMXBs across a broad range of host galaxy masses and environments.

From the *HST* observations of the galaxy, we estimate that 121 globular clusters are present in the region studied, 10 arcsec $< r < r_{\rm ext}$. We find that the cluster system is somewhat bimodal, similar to that of other early-type galaxies. Previous work based on ground-based data and *HST* WFPC2 data for a smaller region did not find evidence for such bimodality, possibly due to smaller samples or increased contamination.

None of the NGC 7457's globular clusters are found to host LMXBs with $L_x > 10^{37}{\rm erg\,s^{-1}}$. Considering other galaxies with similarly deep X-ray observations, we calculate the number of globular cluster LMXBs expected per stellar mass. We find that on average 0.11 and 0.03 LMXBs are observed per $10^6\,{\rm M}_\odot$ in the red and blue globular clusters of these galaxies, respectively. This predicts around three LMXBs in NGC 7457's globular cluster system. Given the small numbers and uncertainties in this prediction, this is consistent with our non-detection.

Nuclear X-ray emission is detected from the relatively low-mass central SMBH. We calculate that the ratio of X-ray to the Eddington luminosity of this source increases from 0.5×10^{-6} to 1.3×10^{-6}. This is the highest $L_x/L_{\rm Edd}$ ratio among the 12 galaxies with 'secure' SMBH masses studied by Gültekin et al. (2012). This is consistent with the idea that lower mass black holes may accrete at higher Eddington fractions than higher mass black holes.

ACKNOWLEDGEMENTS

We thank the referee of this paper, Paolo Bonfini, for providing detailed and informed feedback on the original manuscript. We are very grateful to the CXC helpdesk for providing detailed and helpful advice on the analysis of these merged ACIS data. This research has made use of software provided by the Chandra X-ray Center (CXC) in the application packages CIAO, CHIPS and SHERPA. This research has made use of NASA's Astrophysics Data System.

The scientific results reported in this article are based on observations made by the Chandra X-ray Observatory. Support for this work was provided by NASA through Chandra Award numbers GO5-16084A (MBP) and GO5-16084B (AK) issued by the Chandra X-ray Observatory Center, which is operated by SAO for and on behalf of the National Aeronautics Space Administration under contract NAS8-03060.

Based on observations made with the NASA/ESA *Hubble Space Telescope*, obtained at the Space Telescope Science Institute, which is operated by the Association of Universities for Research in Astronomy, Inc., under NASA contract NAS 5-26555. These observations are associated with programme HST-GO-13942.001-A. Support for programme number HST-GO-13942.001-A was provided by NASA through a grant from the Space Telescope Science Institute, which is operated by the Association of Universities for Research in Astronomy, Incorporated, under NASA contract NAS5-26555.

REFERENCES

Angelini L., Loewenstein M., Mushotzky R. F., 2001, ApJ, 557, L35
Ashman K. M., Bird C. M., Zepf S. E., 1994, AJ, 108, 2348
Bell E. F., de Jong R. S., 2001, ApJ, 550, 212
Bertin E., Arnouts S., 1996, A&AS, 117, 393
Bohlin R. C., 2011, Technical Report, Instrument Science Report, ACS 2011-02. STScI, Baltimore
Brassington N. J. et al., 2008, ApJS, 179, 142
Brassington N. J. et al., 2009, ApJS, 181, 605
Brodie J. P., Strader J., 2006, ARA&A, 44, 193
Cappellari M. et al., 2013, MNRAS, 432, 1709
Chomiuk L., Strader J., Brodie J. P., 2008, AJ, 136, 234
Clark G. W., 1975, ApJ, 199, L143
Coulter D. A. et al., 2016, ApJ, preprint (arXiv:1612.05189)
Davies M. B., Piotto G., de Angeli F., 2004, MNRAS, 349, 129
de Vaucouleurs G., de Vaucouleurs A., Corwin H. G., Jr, Buta R. J., Paturel G., Fouqué P., 1991, Third Reference Catalogue of Bright Galaxies. Springer, New York
Fabbiano G., 2006, ARA&A, 44, 323
Fall S. M., Romanowsky A. J., 2013, ApJ, 769, L26
Fruscione A. et al., 2006, in Silva D. R., Doxsey R. E., eds, Proc. SPIE Conf. Ser. Vol. 6270, Observatory Operations: Strategies, Processes, and Systems. SPIE, Bellingham, p. 62701V
Gallo E., Treu T., Marshall P. J., Woo J.-H., Leipski C., Antonucci R., 2010, ApJ, 714, 25
Gebhardt K. et al., 2003, ApJ, 583, 92
Gültekin K. et al., 2009, ApJ, 698, 198
Gültekin K., Cackett E. M., Miller J. M., Di Matteo T., Markoff S., Richstone D. O., 2012, ApJ, 749, 129
Hargis J. R., Rhode K. L., Strader J., Brodie J. P., 2011, ApJ, 738, 113
Jarrett T. H., Chester T., Cutri R., Schneider S. E., Huchra J. P., 2003, AJ, 125, 525
Jordán A. et al., 2004, ApJ, 613, 279
Jordán A. et al., 2007, ApJ, 671, L117
Kim D.-W., Fabbiano G., 2010, ApJ, 721, 1523
Kim D.-W. et al., 2009, ApJ, 703, 829
Kim D.-W., Fabbiano G., Ivanova N., Fragos T., Jordán A., Sivakoff G. R., Voss R., 2013, ApJ, 764, 98
Kundu A., Maccarone T. J., Zepf S. E., 2002, ApJ, 574, L5
Kundu A., Maccarone T. J., Zepf S. E., 2007, ApJ, 662, 525
Lehmer B. D. et al., 2014, ApJ, 789, 52
Li Z. et al., 2010, ApJ, 721, 1368
Lin D. et al., 2015, ApJ, 808, 20
Luo B. et al., 2013, ApJS, 204, 14
Maraston C., 2005, MNRAS, 362, 799
Muratov A. L., Gnedin O. Y., 2010, ApJ, 718, 1266
Peacock M. B., Zepf S. E., 2016, ApJ, 818, 33
Peacock M. B., Maccarone T. J., Waters C. Z., Kundu A., Zepf S. E., Knigge C., Zurek D. R., 2009, MNRAS, 392, L55
Peacock M. B., Maccarone T. J., Kundu A., Zepf S. E., 2010, MNRAS, 407, 2611
Peacock M. B., Zepf S. E., Maccarone T. J., Kundu A., Gonzalez A. H., Lehmer B. D., Maraston C., 2014, ApJ, 784, 162
Peng E. W. et al., 2006, ApJ, 639, 95
Pooley D. et al., 2003, ApJ, 591, L131
Pota V. et al., 2013, MNRAS, 428, 389
Sivakoff G. R. et al., 2007, ApJ, 660, 1246
Sivakoff G. R., Jordán A., Juett A. M., Sarazin C. L., Irwin J. A., 2008, ApJ, preprint (arXiv:0806.0626)
Strader J., Brodie J. P., Spitler L., Beasley M. A., 2006, AJ, 132, 2333
Taylor M. B., 2006, in Gabriel C., Arviset C., Ponz D., Enrique S., eds, ASP Conf. Ser. Vol. 351, Astronomical Data Analysis Software and Systems XV. Astron. Soc. Pac., San Francisco, p. 666
Tully R. B. et al., 2013, AJ, 146, 86
Verbunt F., Hut P., 1987, in Helfand D. J., Huang J.-H., eds, Proc. IAU Symp. Vol. 125, The Origin and Evolution of Neutron Stars. D. Rediel Publishing Co., Dordrecht, p. 187
Villegas D. et al., 2010, ApJ, 717, 603
Voss R. et al., 2009, ApJ, 701, 471
Zepf S. E., Ashman K. M., 1993, MNRAS, 264, 611
Zhang Z. et al., 2011, A&A, 533, A33

This paper has been typeset from a TEX/LATEX file prepared by the author.